High Temperature, Vol. 33, No. 5, 1995, pp. 732 - 742. Translated from Teplofizika Vysokikh Temperatur, Vol. 33, No. 5, 1995, pp. 738 - 748.

HEAT AND MASS TRANSFER AND PHYSICAL GAS DYNAMICS

Calculation of Statistical Characteristics of Turbulent Flow in a Rotating Round Pipe

A. F. Kurbatskii, S. V. Poroseva, and S. N. Yakovenko

Institute of Theoretical and Applied Mechanics, Siberian Division of the Russian Academy of Sciences, Novosibirsk, Russia
Novosibirsk State University, Novosibirsk, 630090 Russia

Received September 14, 1994

Abstract – Numerical results are given, which characterize the behavior of second- and third-order moments of turbulent characteristics under conditions of developed turbulent flow in a round pipe rotating relative to the longitudinal axis. Turbulent transfer is described with the aid of differential equations of the model of second moments and the model of gradient transfer for third-order correlations. A comparison of the calculation results with the experimentally obtained data indicates that, by and large, the employed models of turbulent transfer adequately describe the suppression of turbulence in rotating turbulent flow.

INTRODUCTION

Turbulent swirling flows often occur in engineering and in the environment. In view of this, the investigation of such flows is of practical interest.

Turbulent transfer in such flows is especially characterized by a substantial decrease of the transfer processes in the radial direction.

The effect of swirling of flow on its statistical characteristics was numerically investigated [1, 2] on the basis of semiempirical equations describing the behavior of fields of average velocity and second moments in the approximation of local equilibrium. It has been demonstrated that the effect of mass forces in swirling flow (centrifugal and Coriolis acceleration) is similar to the effect of acceleration of gravity in a flow with variable density (stratification) and leads to a decrease of the coefficients of momentum and heat transfer.

This paper describes the results of calculations of the first, second and third moments of the velocity field of turbulent flow in a round pipe rotating around the longitudinal axis. The components of the turbulent stress tensor are determined from the differential equations of turbulent transfer (the model of second moments). The model of gradient transfer is used to calculate the third-order moments of the velocity field.

THE MODEL OF SECOND MOMENTS OF THE VELOCITY FIELD

The model designed to describe the behavior of the second-order moments of the velocity field includes the differential equations of turbulent transfer for the mean-velocity vector and the turbulent stress tensor [3 - 5], as well as the differential equations of transfer for the kinetic energy of turbulence E and the rate of its dissipation ε.

The differential equations of turbulent transfer for second moments may yield, in the local balance approximation, algebraic expressions for calculating turbulent stresses. The simplest version is the E–ε model of turbulence in which the Reynolds stress $\langle u_i u_j \rangle$ is calculated on the basis of the model of gradient transfer by the isotropic expression for the coefficient of turbulent viscosity. Note that the E–ε model of turbulence with the isotropic coefficient of turbulent viscosity does not make it possible to reproduce [3], without additional modification, the anisotropy of the components of the turbulent stress tensor $\langle u_i u_j \rangle$.

The effect of suppression of turbulent pulsation characteristics in a swirling flow is allowed for by way of introducing in the ε-equation an additional term that includes the "Richardson number of swirling" [6, 7]. The damping effect of the wall on the transverse pulsations of velocity is included with the aid of corrections to the standard model of [8, 9] for the pressure-velocity shift correlation in the equations defining the second moments. The wall effects are included by way of modifying the destruction terms in the equations for $\langle u_i u_j \rangle$ and ε [10].

In order to describe the flow in a rotating pipe, the cylindrical system of coordinates $x^i = (x, r, \varphi)$ is used, where x is reckoned along the pipe axis, r in the radial direction, and φ in the azimuthal direction. The tensor notation is used for the arbitrary curvilinear system of coordinates. In the cylindrical coordinates, the components of mean and pulsation velocities have the form $U_i = (U, V, rW)$, $U^i = (U, V, W/r)$, $u_i = (u, v, rw)$, $u^i = (u, v, w/r)$. The system of transfer equations for the mean velocity vector and the turbulent stress tensor for steady incompressible flow in the general tensor form

0018-151X/95/3305-0732$12.50 © 1995 МАИК Наука/Interperiodica Publishing

is written as

$$U^i_{,i} = 0, \quad U^j U_{i,j} = \nu g^{jk} U_{i,jk} - \langle u_i u^j \rangle_{,j} - \hat{p}_{,i}/\rho, \tag{1}$$

$$U^k \langle u_i u_j \rangle_{,k} = \nu \left(g^{km} \langle u_i u_j \rangle_{,k} \right)_{,m} + D_{ij} + P_{ij} + \pi_{ij} - \varepsilon_{ij}, \tag{2}$$

where $D_{ij} = -\langle u_i u_j u^m \rangle_{,m} - (\langle pu_i \rangle_{,j} + \langle pu_j \rangle_{,i})/\rho$ is turbulent transfer, $P_{ij} = -\langle u_j u^k \rangle U_{i,k} - \langle u_i u^k \rangle U_{j,k}$ is generation, $\pi_{ij} = \langle p(u_{i,j} + u_{j,i}) \rangle/\rho$ is the pressure-velocity shift correlation, and $\varepsilon_{ij} = 2\nu g^{km} \langle u_{i,m} u_{j,k} \rangle$ is dissipation. In equations (1) and (2), the symbols ",i" denote covariant differentiation with respect to the coordinate x^i, g^{ij} is the metric tensor, $\langle \ldots \rangle$ denotes time averaging, p is the pressure, ρ is the density, and ν is the kinematic viscosity coefficient.

In order to derive the closed form of system (1) and (2), one needs model representations for the terms D_{ij}, π_{ij}, and ε_{ij}. The simplest model expression of the gradient type for the processes of turbulent diffusion (third-order moments) may be written as [11]

$$-\langle u_i u_j u^m \rangle = -g^{km} \langle u_i u_j u_k \rangle = g^{km} c_s \frac{E}{\varepsilon} \langle u_k u^\alpha \rangle \langle u_i u_j \rangle_{,\alpha}. \tag{3}$$

Here, $c_s = 0.18$ is an empirical coefficient. The equation for the kinetic energy of turbulence, derived from the convolution of equation (2) in view of (3), has the form

$$U^k E_{,k} = \left[g^{km} \left(\nu E_{,k} + c_s \frac{E}{\varepsilon} \langle u_k u^\alpha \rangle E_{,\alpha} \right) \right]_{,m} + P - \varepsilon - \frac{2\nu E}{x_n^2}, \tag{4}$$

where $E = (1/2)\langle u_i u^i \rangle$, $P = -(1/2)[\langle u_i u^k \rangle U^i_{,k} + \langle u^i u^k \rangle U_{i,k}]$ is the generation of the turbulence energy, and ε is dissipation. The latter term appears in (4) as the result of including the effect of low Reynolds numbers near the wall in the standard expression for $\varepsilon_{ij} = 2/3\delta_{ij}\varepsilon$ [10],

$$\varepsilon_{ij} = \frac{2}{3} g_{ij} \varepsilon + 2\nu \frac{\langle u_i u_j \rangle}{x_n^2}, \tag{5}$$

where x_n is the distance to the wall.

The pressure-velocity shift correlation is represented [5] as the sum of three terms,

$$\pi_{ij} = \pi^{(1)}_{ij} + \pi^{(2)}_{ij} + (\pi'^{(1)}_{ij} + \pi'^{(2)}_{ij}) f(x_n). \tag{6}$$

The first term describes the tendency of turbulence to isotropic state in the absence of the mean velocity shift and wall effect,

$$\pi^{(1)}_{ij} = -c_1 \frac{\varepsilon}{E} \left(\langle u_i u_j \rangle - \frac{2}{3} g_{ij} E \right) \quad (c_1 = 1.5), \tag{7}$$

the second term describes the contribution of the mean velocity gradient,

$$\pi^{(2)}_{ij} = -c_2 (P_{ij} - 2/3 g_{ij} P) \quad (c_2 = 0.6), \tag{8}$$

and the third term describes the wall effect [9],

$$\pi'^{(1)}_{ij} = c'_1 \frac{\varepsilon}{E} [\langle u_n^2 \rangle g_{ij} - 3/2 (\langle u_n u_j \rangle g_{in} + \langle u_n u_i \rangle g_{jn})], \tag{9}$$

$$\pi'^{(2)}_{ij} = c'_2 [\pi^{(2)}_{nn} g_{ij} - 3/2 (\pi^{(2)}_{nj} g_{in} + \pi^{(2)}_{ni} g_{jn})] \tag{10}$$

with the damping function $f = (1/5)E^{3/2}/(\varepsilon x_n)$, where the subscript n indicates the direction on a normal to the wall ($c'_1 = c'_2 = 0.3$).

The quantity ε, entering the model expressions, is determined from the approximately closed differential equation of transfer

$$U^k \varepsilon_{,k} = \left[g^{km} \left(\nu \varepsilon_{,k} + c_\varepsilon \frac{E}{\varepsilon} \langle u_k u^\alpha \rangle \varepsilon_{,\alpha} \right) \right]_{,m} + \{ c_{\varepsilon 1} P - c^*_{\varepsilon 2} \varepsilon \} \frac{\varepsilon}{E} - \frac{2\nu\varepsilon}{x_n^2} f_1, \tag{11}$$

where the function $f_1 = \exp(-0.5 x_n u_* / \nu)$, $c_\varepsilon = 0.18$, $c_{\varepsilon 1} = 1.35$, $c_{\varepsilon 2} = 1.8$, $c^*_{\varepsilon 2} = \max[1.4, c_{\varepsilon 2} f_2 (1 - c_{\varepsilon 3} \mathrm{Ri}_W)]$, and $f_2 = 1 - 2/9 \exp[-(E^2/(6\nu\varepsilon))^2]$.

The Richardson number of swirling Ri_W in (11) describes the effect of the curvature of the lines of flow on turbulence by analogy with the effect of stratification of the medium on turbulent transfer [6]. The curvature of the lines of flow is included in the destruction term in (11). The expression for the number $\mathrm{Ri}_W = [(W/r)/(\partial W/\partial r)]/ /[(\partial U/\partial r)^2 + (\partial W/\partial r)^2]$ is written as in [7], by analogy with the Richardson number in stratified turbulent flows [3, 9]. The modification of the destruction term in equation (11) is based on the hypothesis that the stabilizing effect of swirling may be included in terms of the linear scale of turbulent vortexes $L(=E/\varepsilon)$, which decreases at $\mathrm{Ri}_W > 0$, i.e., in terms of the increase of dissipation ε that leads to suppression of the turbulence energy E. The magnitude of the coefficient $c^*_{\varepsilon 2}$ is assumed to be restricted from below ($c^*_{\varepsilon 2} \geq 1.4$) so that the dissipation ε should not become "too great" because of the decrease of the coefficient $c_{\varepsilon 2} f_2 (1 - c_{\varepsilon 3} \mathrm{Ri}_W)$ with a rise of Ri_W during the increase of the rate of pipe rotation W_0. The value of the coefficient $c_{\varepsilon 3} = 2.0$ is found by numerical optimization.

Model representations (5) - (11), formulated above, lead to a closed system of equations of turbulent transfer for first and second moments. For a steady axisymmetric pipe flow, the equations of the model in the

cylindrical coordinates take the form

$$\frac{\partial U}{\partial x} + \frac{1}{r}\frac{\partial}{\partial r}(rV) = 0, \tag{12}$$

$$U\frac{\partial U}{\partial x} + V\frac{\partial U}{\partial r} = \frac{1}{r}\frac{\partial}{\partial r}\left[r\left(\nu\frac{\partial U}{\partial r} - \langle uv\rangle\right)\right] - \frac{1}{\rho}\frac{\partial \hat{p}}{\partial x}, \tag{13}$$

$$U\frac{\partial W}{\partial x} + V\frac{\partial W}{\partial r} + V\frac{W}{r} = \frac{1}{r}\frac{\partial}{\partial r}\left[r\left(\nu\frac{\partial W}{\partial r} - \langle vw\rangle\right)\right] - \nu\frac{W}{r^2} - \frac{\langle vw\rangle}{r}, \tag{14}$$

$$U\frac{\partial E}{\partial x} + V\frac{\partial E}{\partial r} = \frac{1}{r}\frac{\partial}{\partial r}\left[r\left(\nu + c_s\frac{E}{\varepsilon}\langle v^2\rangle\right)\frac{\partial E}{\partial r}\right] + P - \varepsilon - \frac{2\nu E}{(R-r)^2}, \tag{15}$$

$$U\frac{\partial \varepsilon}{\partial x} + V\frac{\partial \varepsilon}{\partial r} = \frac{1}{r}\frac{\partial}{\partial r}\left[r\left(\nu + c_\varepsilon\frac{E}{\varepsilon}\langle v^2\rangle\right)\frac{\partial \varepsilon}{\partial r}\right] + \{c_{\varepsilon 1}P - c^*_{\varepsilon 2}\varepsilon\}(\varepsilon/E) - [2\nu\varepsilon/(R-r)^2]f_1, \tag{16}$$

where U, V, and W are the components of the mean velocity vector in the longitudinal, radial, and azimuthal directions, respectively; and u, v, and w are the respective pulsation components of velocity. The turbulent stresses that enter equations (13) - (16) are found from differential transfer equations (2) approximately closed in accordance with expressions (3), (5) - (10). For individual components of the stress tensor, these equations are written as

$$U\frac{\partial\langle u^2\rangle}{\partial x} + V\frac{\partial\langle u^2\rangle}{\partial r} = \frac{1}{r}\frac{\partial}{\partial r}\left[r\left(\nu + c_s\frac{E}{\varepsilon}\langle v^2\rangle\right)\frac{\partial\langle u^2\rangle}{\partial r}\right] + P_{11} + \{-c_1\frac{\varepsilon}{E}(\langle u^2\rangle - \frac{2}{3}E) - c_2(P_{11} - \frac{2}{3}P) + \pi' f\} - \frac{2}{3}\varepsilon - \frac{2\nu}{(R-r)^2}\langle u^2\rangle, \tag{17}$$

$$U\frac{\partial\langle v^2\rangle}{\partial x} + V\frac{\partial\langle v^2\rangle}{\partial r} - 2\langle vw\rangle\frac{W}{r} = \frac{1}{r}\frac{\partial}{\partial r}\left[r\left(\nu + c_s\frac{E}{\varepsilon}\langle v^2\rangle\right)\frac{\partial\langle v^2\rangle}{\partial r}\right] - \frac{2}{r}c_s\left[\frac{\partial}{\partial r}\left(\frac{E}{\varepsilon}\langle vw\rangle\langle vw\rangle\right) + \frac{E}{\varepsilon}\langle vw\rangle\frac{\partial\langle vw\rangle}{\partial r}\right] + 2\left(\nu + c_s\frac{E}{\varepsilon}\langle w^2\rangle\right)\frac{\langle w^2\rangle - \langle v^2\rangle}{r^2} + P_{22} + \{-c_1\frac{\varepsilon}{E}(\langle v^2\rangle - \frac{2}{3}E) - c_2(P_{22} - \frac{2}{3}P) - 2\pi' f\} - \frac{2}{3}\varepsilon - \frac{2\nu}{(R-r)^2}\langle v^2\rangle, \tag{18}$$

$$U\frac{\partial\langle w^2\rangle}{\partial x} + V\frac{\partial\langle w^2\rangle}{\partial r} = \frac{1}{r}\frac{\partial}{\partial r}\left[r\left(\nu + c_s\frac{E}{\varepsilon}\langle v^2\rangle\right)\frac{\partial\langle w^2\rangle}{\partial r}\right] + \frac{2}{r}c_s\left[\frac{\partial}{\partial r}\left(\frac{E}{\varepsilon}\langle vw\rangle\langle vw\rangle\right) + \frac{E}{\varepsilon}\langle vw\rangle\frac{\partial\langle vw\rangle}{\partial r}\right] - 2\langle vw\rangle\frac{W}{r} - 2\left(\nu + c_s\frac{E}{\varepsilon}\langle w^2\rangle\right)\frac{\langle w^2\rangle - \langle v^2\rangle}{r^2} + P_{33} + \{-c_1\frac{\varepsilon}{E}(\langle w^2\rangle - \frac{2}{3}E) - c_2(P_{33} - \frac{2}{3}P) + \pi' f\} - \frac{2}{3}\varepsilon - \frac{2\nu}{(R-r)^2}\langle w^2\rangle, \tag{19}$$

$$U\frac{\partial\langle uv\rangle}{\partial x} + V\frac{\partial\langle uv\rangle}{\partial r} - \langle uw\rangle\frac{W}{r} = \frac{1}{r}\frac{\partial}{\partial r}\left[r\left(\nu + c_s\frac{E}{\varepsilon}\langle v^2\rangle\right)\frac{\partial\langle uv\rangle}{\partial r}\right] - \frac{c_s}{r}\left[\frac{\partial}{\partial r}\left(\frac{E}{\varepsilon}\langle vw\rangle\langle uw\rangle\right) + \frac{E}{\varepsilon}\langle vw\rangle\frac{\partial\langle uw\rangle}{\partial r}\right] - \left(\nu + c_s\frac{E}{\varepsilon}\langle w^2\rangle\right)\frac{\langle uv\rangle}{r^2} + P_{12} + \{-c_1\frac{\varepsilon}{E}\langle uv\rangle - c_2P_{12} - \frac{3}{2}(c_1'\frac{\varepsilon}{E}\langle uv\rangle + c_2'c_2P_{12})f\} - \left[\frac{2\nu}{(R-r)^2}\right]\langle uv\rangle, \tag{20}$$

$$U\frac{\partial\langle vw\rangle}{\partial x} + V\frac{\partial\langle vw\rangle}{\partial r} - [\langle w^2\rangle - \langle v^2\rangle]\frac{W}{r} = \frac{1}{r}\frac{\partial}{\partial r}\left[r\left(\nu + c_s\frac{E}{\varepsilon}\langle v^2\rangle\right)\frac{\partial\langle vw\rangle}{\partial r}\right] - \frac{c_s}{r}\left[\frac{\partial}{\partial r}\left(\frac{E}{\varepsilon}\langle vw\rangle(\langle w^2\rangle - \langle v^2\rangle)\right) + \frac{E}{\varepsilon}\langle vw\rangle\frac{\partial}{\partial r}(\langle w^2\rangle - \langle v^2\rangle) - 4\left(\nu + c_s\frac{E}{\varepsilon}\langle w^2\rangle\right)\frac{\langle vw\rangle}{r^2} + P_{23} + \{-c_1\frac{\varepsilon}{E}\langle vw\rangle - c_2P_{23} - \frac{3}{2}(c_1'\frac{\varepsilon}{E}\langle vw\rangle + c_2'c_2P_{23})f\} - \left[\frac{2\nu}{(R-r)^2}\right]\langle vw\rangle, \tag{21}$$

$$U\frac{\partial\langle uw\rangle}{\partial x}+V\frac{\partial\langle uw\rangle}{\partial r}+\langle uv\rangle\frac{W}{r}$$
$$=\frac{1}{r}\frac{\partial}{\partial r}\left[r\left(\nu+c_s\frac{E}{\varepsilon}\langle v^2\rangle\right)\frac{\partial\langle uw\rangle}{\partial r}\right]$$
$$+\frac{c_s}{r}\left[\frac{\partial}{\partial r}\left(\frac{E}{\varepsilon}\langle vw\rangle\langle uv\rangle\right)+\frac{E}{\varepsilon}\langle vw\rangle\frac{\partial\langle uv\rangle}{\partial r}\right] \quad (22)$$
$$-\left(\nu+c_s\frac{E}{\varepsilon}\langle w^2\rangle\right)\frac{\langle uw\rangle}{r^2}+P_{13}+$$
$$+\left\{-c_1\frac{E}{\varepsilon}\langle uw\rangle-c_2P_{13}\right\}-\left[\frac{2\nu}{(R-r)^2}\right]\langle uw\rangle,$$

$$\pi'=c_1'\frac{\varepsilon}{E}\langle v^2\rangle-c_2'c_2\left(P_{22}-\frac{2}{3}P\right),$$

$$f=\frac{1}{5}\frac{E^{3/2}/\varepsilon}{(R-r)},$$

$$P_{11}=-2\langle uv\rangle\frac{\partial U}{\partial r},\quad P_{22}=2\langle vw\rangle\frac{W}{r},$$

$$P_{33}=-2\langle vw\rangle\frac{\partial W}{\partial r},$$

$$\hat{P}=\frac{1}{2}\left(P_{11}+P_{22}+P_{33}\right),$$

$$P_{12}=-\langle v^2\rangle\frac{\partial U}{\partial r}+\langle uw\rangle\frac{W}{r},$$

$$P_{23}=-\langle v^2\rangle\frac{\partial W}{\partial r}+\langle w^2\rangle\frac{W}{r},$$

$$P_{13}=-\langle uv\rangle\frac{\partial W}{\partial r}-\langle vw\rangle\frac{\partial U}{\partial r}.$$

For convenience of numerical realization, equation (15) for $E=1/2(\langle u^2\rangle+\langle v^2\rangle+\langle w^2\rangle)$ and the equation for $\alpha\equiv\langle w^2\rangle-\langle v^2\rangle$, derived from (18) and (19), were used instead of equations (18) and (19) for $\langle v^2\rangle$ and $\langle w^2\rangle$. The latter substitution is due to the presence in the equations for $\langle v^2\rangle$ and $\langle w^2\rangle$ of a singularity on the pipe axis because of the source of the form $\pm2(\nu+c_s(E/\varepsilon)\langle w^2\rangle)\alpha/r^2$ if $\alpha\neq0$. The values of $\langle v^2\rangle$ and $\langle w^2\rangle$ are determined from the quantities E, $\langle u^2\rangle$, and α, found from the transfer equations: $\langle v^2\rangle=E-(\langle u^2\rangle+\alpha)/2$.

The pressure gradient $-1/\rho(dP/dx)$ in equation (13) is found from the condition of conservation of flow rate in the form

$$-\frac{1}{\rho}\frac{d\hat{p}}{dx}=\frac{2}{R^2}\left[-r\left(\nu\frac{\partial U}{\partial r}-\langle uv\rangle\right)\right]_0^R$$
$$=\frac{2\nu}{R}\left(-\frac{\partial U}{\partial r}\right)_{r=R}.$$

At the inlet to the rotating section of the pipe, the pressure gradient $-1/\rho(d\hat{p}/dx)=2(u_{*0}^2/R)$ is known (u_{*0} is the friction velocity on the pipe wall in developed turbulent flow delivered to the rotating section). The friction velocity in the rotating section of the pipe is found from the expression

$$u_*=\left[\nu\left(\frac{\partial U}{\partial r}\right)_{r=R}\right]^{1/2}.$$

The values of the numerical coefficients of the model of second moments (12) - (22) c_1, c_2, c_1', c_2', $c_{\varepsilon1}$, $c_{\varepsilon2}$, c_ε, and c_s correspond to their "standard" values [3, 5, 9, 10].

The boundary conditions for the differential transfer equations of the model of second moments take the following form:

for $r=0$ (on the pipe axis)

$$\frac{\partial U}{\partial r}=\frac{\partial E}{\partial r}=\frac{\partial\varepsilon}{\partial r}=\frac{\partial\langle u^2\rangle}{\partial r}=\frac{\partial\alpha}{\partial r}$$
$$=\langle uv\rangle=\langle vw\rangle=\langle uw\rangle=W=0,$$

and for $r=R$ (on the pipe wall)

$$U=E=\varepsilon=\langle u^2\rangle=\alpha=\langle uv\rangle=\langle vw\rangle=\langle uw\rangle=0,$$
$$W=W_0>0.$$

The determining system of parabolic equations for U, W, E, ε, and $\langle u_iu_j\rangle$ was solved by the test volume method [12].

The calculations were performed in two stages, namely: (1) derivation of developed flow without swirling, and (2) superposition on the developed flow of the pipe rotation at the velocity W_0.

At the first stage of calculation, the initial velocity profile was preassigned in the form of combination of the linear function $U(r)=u_*y^+$ for $0\le y^+\le y_R^+$ and the power function $U(r)=Au_{*0}(y^+)^{1/7}$ for $y_R^+<y^+\le\mathrm{Re}^*$, where $y^+=(R-r)u_{*0}/\nu$, $\mathrm{Re}^*=Ru_{*0}/\nu$, $A=8.74$, and $y_R^+=A^{7/6}$. The magnitudes of the turbulence energy and its components were taken to be equal to small background values: $E(r)=E_0=10^{-3}u_*^2$, $\langle u^2\rangle=\frac{2}{3}E_0$, $\alpha=0$, $\langle uv\rangle|_{x=0}=0$. The dissipation of energy $\varepsilon(r)=\sqrt{c_\mu f_\mu}E_0(\partial U/\partial r)$ was found from the assumptions of local equilibrium ($P=\varepsilon$) and gradient coupling ($\langle uv\rangle=-c_\mu f_\mu\frac{E^2}{\varepsilon}\frac{\partial U}{\partial r}$, where $c_\mu=0.09$ and the damping function $f_\mu=1-\exp(-0.01y^+)$ are borrowed from [10]): $\varepsilon(r)=\sqrt{c_\mu f_\mu}E_0(\partial U/\partial r)$; $\langle uv\rangle|_{x=0}=0$.

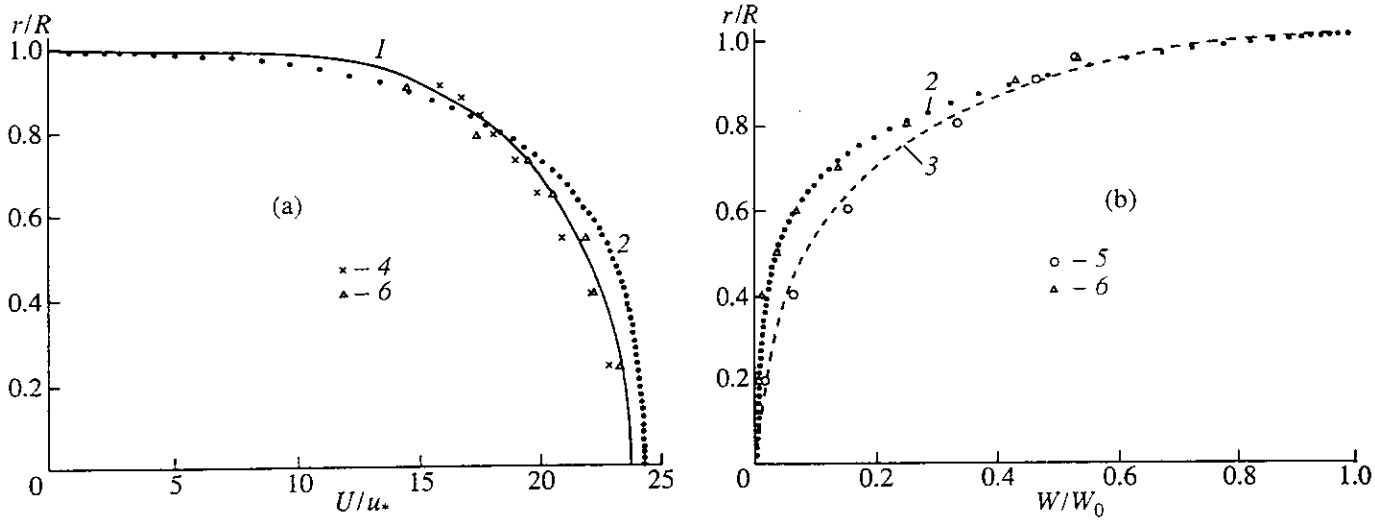

Fig. 1. Profiles of mean velocity components: (a) U and (b) W for different values of the swirling parameter Π Calculation of Π: *1* – 0, *2* – 0.6, *3* – 0.15. Experimental data of [13]: *4* – $\Pi = 0$, *5* – 0.15, *6* – 0.6.

At the second stage of calculation, the input data were provided by the transverse profiles of U, E, ε, $\langle u^2 \rangle$, $\alpha \equiv \langle w^2 \rangle - \langle v^2 \rangle$, and $\langle uv \rangle$, derived at the first stage and corresponding to developed turbulent flow in a pipe. The remaining sought functions were taken equal to $W(r = R) = W_0$, $W(r < R) = \langle vw \rangle = \langle uw \rangle = 0$.

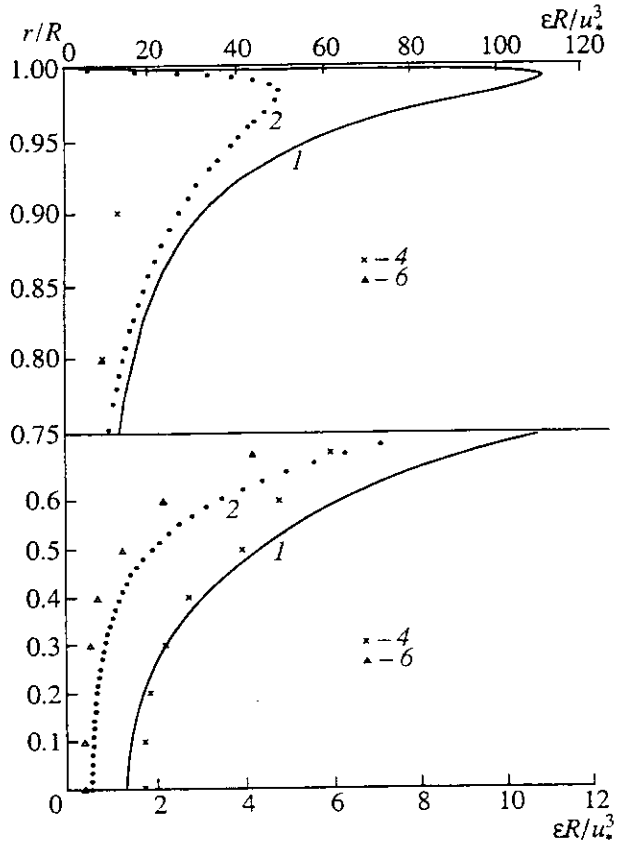

Fig. 2. Profiles of dissipation of the kinetic energy of turbulence (designations are the same as in Fig. 1).

The calculated characteristics have been made dimensionless with the aid of the dynamic velocity u_{*0} and the pipe radius R. The inlet parameter Re* = 875, as in the experiment of [13], with whose data the calculation results are compared (R = 3 cm, $U_0 = 10^3$ cm/s, $\nu = 0.149$ cm^2/s, $u_{*0} = 43.5$ cm/s). At the first stage of calculation, the results were obtained for the distance of 200R on the x-coordinate along the pipe axis, and at the second stage for 50R, as in the experiment. The establishment of flow with an increase of x may be characterized by the magnitude of advection of the turbulence energy, decreasing at the end of the first stage of calculation to a negligibly small value: $|U(\partial E/\partial x)|_{\max} \sim 10^{-2} u_{*0}^3/R \ll \varepsilon_{\min}$. At the end of the second stage of calculation, the relative magnitude of advection is much higher, and no establishment of turbulent flow characteristics with respect to x was observed.

RESULTS OF CALCULATION OF FIRST- AND SECOND-ORDER MOMENTS OF VELOCITY FIELD

The results of numerical experiments for flow in a rotating pipe with different swirling parameters are given in Figs. 1 - 6 for the pipe cross section $x/R = 50$. The dots indicate the experimental data of [13], and the curves correspond to the results of calculation according to the model of second moments.

In the experiments of Zaets *et al.* [13], with whose data the calculation results are compared, swirling flow was produced according to the following scheme. Developed turbulent flow from the nonrotating section of a straight round pipe 100-caliber long was delivered to a pipe section 25-caliber long rotating around the longitudinal axis at a constant angular velocity. The measurements were performed in the exit section of the

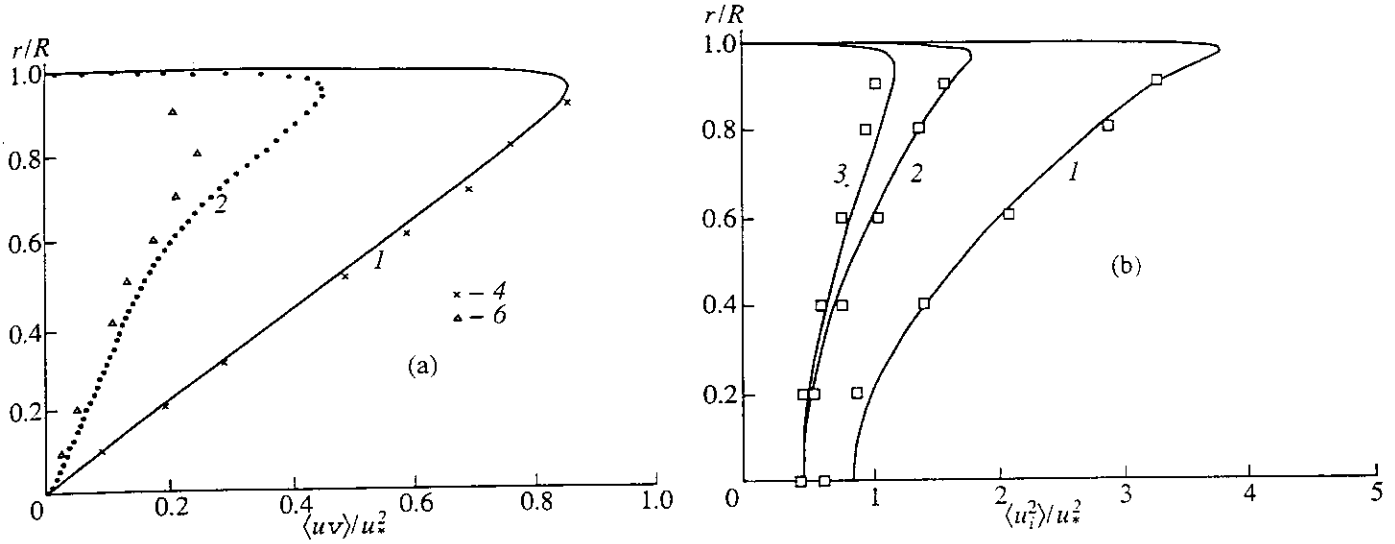

Fig. 3. Profiles of (a) tangential $\langle uv \rangle$ and (b) normal components of turbulent Reynolds stresses: (a) designations are the same as in Fig. 1; (b) $1 - \langle u^2 \rangle$, $2 - \langle v^2 \rangle$, $3 - \langle w^2 \rangle$.

rotating section for the Reynolds number $\mathrm{Re}_D = (U_0 2R)/\nu = 4 \times 10^4$. The degree of swirling of flow is characterized by the swirling parameter $\Pi = W_0/U_0 = \omega_0 R/U_0$, where ω_0 is the angular velocity of pipe rotation, U_0 is the velocity of flow on the pipe axis, and R is the pipe radius. The swirling parameter of flow Π was varied by varying the rotation frequency of the channel.

In the case of nonswirling flow, the results of measurements [13] of the longitudinal component of mean velocity, Reynolds stresses, turbulence energy, and the rate of its dissipation adequately agree with the data known from literature [14 - 16]. The experimental profile of $U(r)$ for $\Pi = 0$ (Fig. 1a) is approximately described by the power relation. The results of measurements of dissipation $\varepsilon(r)$ for $\Pi = 0$ are well reproduced by the model in the $0.2 < r < 0.6$ range (Fig. 2). The model fairly adequately describes the behavior of the components of turbulent stresses (Fig. 3a) and, in particular, the anisotropy of normal stresses both in the vicinity of the wall and on the flow axis, where $\langle v^2 \rangle = \langle w^2 \rangle$ и $\langle u^2 \rangle \approx 2\langle v^2 \rangle$ (Fig. 3b), that is observed in the experiments.

When swirling is superposed on developed turbulent flow with a constant air flow rate, some increase of the longitudinal component of mean velocity in the axis zone (for $0 \le \Pi \le 0.6$) is observed (Fig. 1a) both in calculations and in the experiment. The $U(r)$ profile is deformed under the centrifugal force: the slope of the profile ($\partial U/\partial r$ derivative) near the wall decreases, which points to the decrease of turbulent friction as the swirling of flow increases.

As the rotation frequency of the pipe increases, the relative magnitude of the azimuthal component of mean velocity W/W_0 in the axis region decreases (Fig. 1b). As the swirling parameter Π increases, the $W(r)$ distribution becomes ever more nonuniform on the radius (in the exit cross section of the rotating section of the pipe). As seen from the drawing, the model of second moments well describes the behavior of azimuthal velocity W/W_0 for the greatest value of the swirling parameter $\Pi = 0.6$.

The model of turbulence, employed by us, reproduces the experimentally observed effect of the decrease of the pulsation characteristics of E, ε, and $\langle u_i u_j \rangle$ as the swirling parameter increases (mainly, in the axis region). In so doing, the behavior of the turbulence energy (Fig. 4), the rate of its dissipation (Fig. 2) and tangential stresses (Fig. 3a) outside of the wall region of flow are also in adequate agreement with the experimental data. The anisotropy of the turbulence energy components, observed in nonswirling flow (Fig. 3b), by

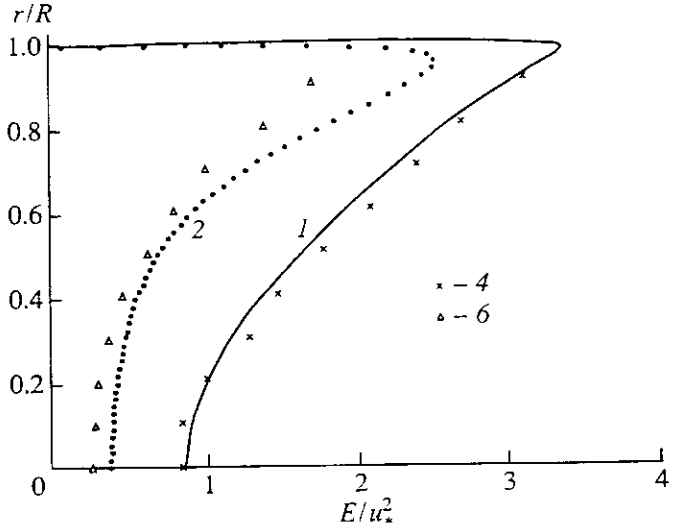

Fig. 4. Profiles of the kinetic energy of turbulence $E = 1/2\langle u_i u_i \rangle$; designations are the same as in Fig. 1.

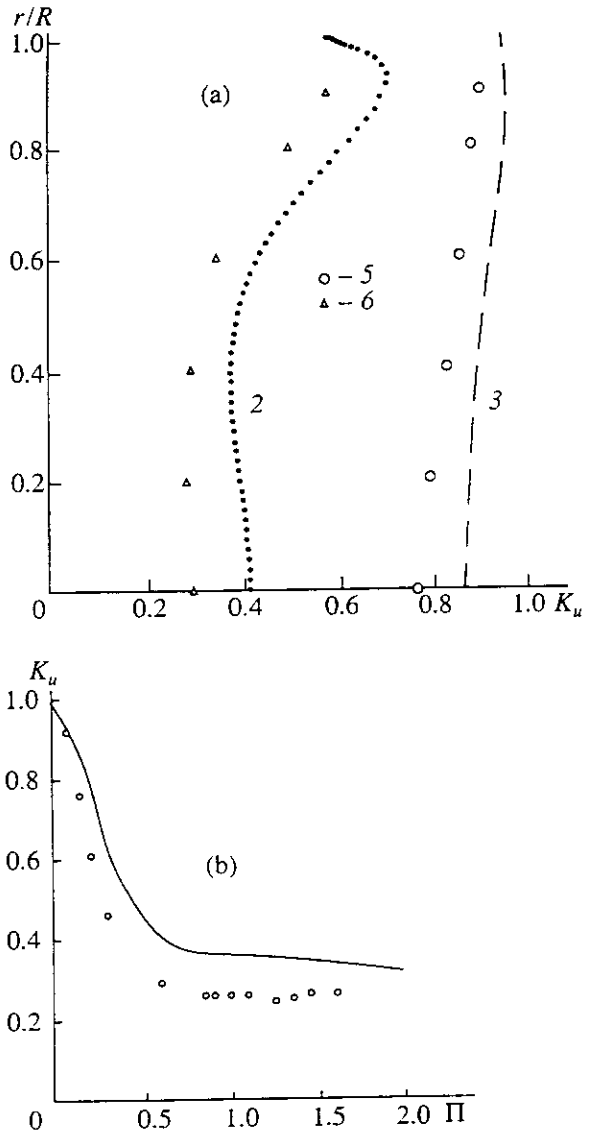

Fig. 5. The suppression coefficient for the longitudinal component of turbulence intensity: (a) K_u profiles (designations are the same as in Fig. 1); (b) K_u as a function of the swirling parameter Π; dots indicate the experimental data of [13].

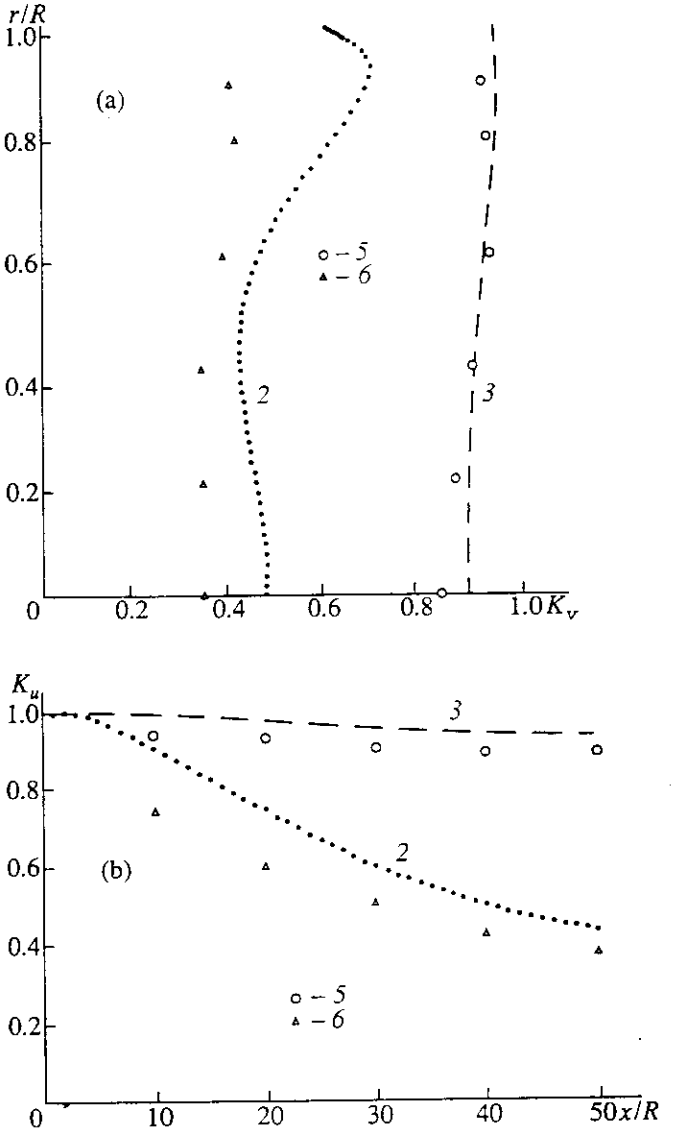

Fig. 6. The suppression coefficient K_u as a function of r and K_u as a function of the longitudinal coordinate: (a) $K_v(r)|_{x=50R}$; (b) K_u ($r = 0.6R$, x); designations are the same as in Fig. 1.

and large persists in the presence of swirling, both in experiments and in calculations.

The effect of swirling of flow on the components of normal stresses $\langle u_i^2 \rangle$ was estimated by the "coefficient of suppression" $K_i = \langle u_i^2 \rangle(\Pi > 0)/\langle u_i^2 \rangle(\Pi = 0)$ of the ith root-mean-square pulsations of velocity. Under conditions of weak swirling ($\Pi \leq 0.3$), the greatest suppression of the pulsation intensity is observed on the flow axis. As the swirling increases (for $\Pi \geq 0.6$), the suppression maximum shifts to the $0.3 \leq r/R \leq 0.6$ region. The model reproduces these effects (Figs. 5 and 6). The calculated transverse profiles of $K_i(r)$ prove to be closest to the measured values (for $\Pi = 0.6$) outside of the axis region. A decrease in suppression is observed in the range of transverse coordinate values of $0.6 \leq r/R \leq 0.9$. The model only qualitatively reproduces the behavior of K_v for $\Pi = 0.6$ and overestimates the values of the suppression coefficients under conditions of weak swirling ($\Pi \leq 0.3$).

The latter remark appears to be also true of the behavior of the dependence of K_u (for $r/R = 0$) on the swirling parameter Π (Fig. 5b). However, the behavior of calculated curves, by and large, corresponds to that observed in experiments; in particular, the suppression of pulsation intensity decreases as the swirling parameter increases (above $\Pi = 0.65$).

The marching procedure of stepwise integration by test volumes, realized during numerical simulation, enables one to follow the variation of flow characteris-

tics with the increase of the longitudinal coordinate x. As the coordinate x increases, the magnitude of the suppression coefficient exhibits the same behavior as in the experiment, i.e., a tendency to saturation both along the pipe (Fig. 6) and with respect to the swirling parameter. For $r/R = 0.6$, this tendency is more evident and closer (with respect to x) to the beginning of the rotating section of the pipe. The effect of swirling in this case starts showing up at the distance $x/R \simeq 4$ - 5 from the beginning, while on the pipe axis, it shows up at the distance $x/R \simeq 10$ - 14. Therefore, the flow is not subjected to the effect of swirling in some convergent cone at the initial part of the rotating section. Theory produces a later (with respect to x) deviation from the value of $K_u = 1$ at the beginning of the section than the experiment.

Therefore, the superposition of swirling on turbulent flow leads to restructuring of the flow characteristics. In a flow of gas in a rotating pipe, suppression occurs under conditions of minor and moderate swirling of flow of radial turbulent transfer, i.e., a decrease of the turbulence energy, its dissipation and turbulent stresses mainly in the axis region of the channel. The flow parameters vary appreciably over the entire length of the rotating section ($0 \le x/R \le 50$). However, both in the experiment and calculations, the results depend on a further increase of the distance from the inlet section.

THE MODEL FOR THIRD-ORDER MOMENTS OF THE VELOCITY FIELD AND THEIR CALCULATION

The model for describing the processes of turbulent diffusion (third moments) is derived from an exact nonclosed equation of transfer for third-order moments in the local balance approximation.

The complete equation for third-order moments in the tensor form is written as

$$U^m \langle u_i u_j u_k \rangle_{,m} = P_{ijk}^{(T)} + P_{ijk}^{(M)} + D_{ijk} + \pi_{ijk} - \varepsilon_{ijk}, \tag{23}$$

where the turbulence generation term

$$P_{ijk}^{(T)} = [\langle u_j u_k \rangle \langle u^m u_i \rangle_{,m} + \langle u_k u_i \rangle \langle u^m u_j \rangle_{,m} + \langle u_i u_j \rangle \langle u^m u_k \rangle_{,m}],$$

is determined in the following form:

generation by mean shift

$$P_{ijk}^{(M)} = -[\langle u_j u_k u^m \rangle U_{i,m} + \langle u_k u_i u^m \rangle U_{j,m} + \langle u_i u_j u^m \rangle U_{k,m}],$$

turbulent and molecular diffusion

$$D_{ijk} = -[\langle u_i u_j u_k u^m \rangle - \nu g^{nm} \langle u_i u_j u_k \rangle_{,n}],$$

pressure effects

$$\pi_{ijk} = \frac{1}{\rho} [\langle p_{,j} u_j u_k \rangle + \langle p_{,j} u_k u_i \rangle + \langle p_{,k} u_i u_j \rangle],$$

and dissipation

$$\varepsilon_{ijk} = 2\nu g^{nm} [\langle u_i u_{j,n} u_{k,m} \rangle + \langle u_{i,n} u_j u_{k,m} \rangle + \langle u_{i,n} u_{j,n} u_k \rangle].$$

The complete model is derived from equation (23), disregarding advection and viscous diffusion:

$$P_{ijk}^{(T)} + P_{ijk}^{(M)} + D_{ijk} + \pi_{ijk} - \varepsilon_{ijk} = 0. \tag{24}$$

Note that Panchapakesan and Lumley [17] have shown that, in the case of a round jet, the advective terms are small as compared with the other terms in equation (24).

For closure of equation (24), the following model representations are employed for some terms. The pressure-velocity shift correlation π_{ijk} is represented, by analogy with the like correlation π_{ij} in the balance equation for Reynolds stresses, as the sum of two parts [18]

$$\pi_{ijk} = \pi_{ijk}^{(1)} + \pi_{ijk}^{(2)}, \tag{25}$$

where $\pi_{ijk}^{(1)} = -c_{f1} P_{ijk}^{(M)}$ allows for generation by mean shift, and

$$\pi_{ijk}^{(2)} = -(1/c_{f3}) \langle u_i u_j u_k \rangle \frac{\varepsilon}{E} - c_{f2} P_{ijk}^{(T)} \tag{26}$$

allows for relaxation of third moments (tendency to isotropy).

The hypothesis of gradient transfer [18] is used for ε_{ijk}:

$$\varepsilon_{ijk} \sim -\frac{E}{\varepsilon} [\langle u_k u_\alpha \rangle \varepsilon_{ij,\alpha} + \langle u_j u_\alpha \rangle \varepsilon_{ik,\alpha} + \langle u_i u_\alpha \rangle \varepsilon_{jk,\alpha}],$$

where $\varepsilon_{ij} = 2\nu \langle u_{i,m} u_{j,m} \rangle$. In view of the assumption of local isotropy for $\varepsilon_{ij} = 2/3 g_{ij} \varepsilon$, the resultant expression for the dissipative term has the form

$$\varepsilon_{ijk} = -c_{\varepsilon 3} \frac{E}{\varepsilon} \varepsilon_{,m} [\langle u_k u^m \rangle g_{ij} + \langle u_j u^m \rangle g_{ki} + \langle u_i u^m \rangle g_{jk}]. \tag{27}$$

Fourth-order moments are expressed in terms of second-order moments by Millionshchikov's hypothesis of quasi-normality,

$$\langle u_i u_j u_k u^m \rangle = \langle u_j u_k \rangle \langle u^m u_i \rangle + \langle u_i u_j \rangle \langle u^m u_k \rangle + \langle u_k u_i \rangle \langle u^m u_j \rangle. \tag{28}$$

Although the probability distribution of turbulent pulsations of velocity is not Gaussian for a round pipe flow, the use of the quasi-normality hypothesis is based on the assumption that the errors, introduced by this

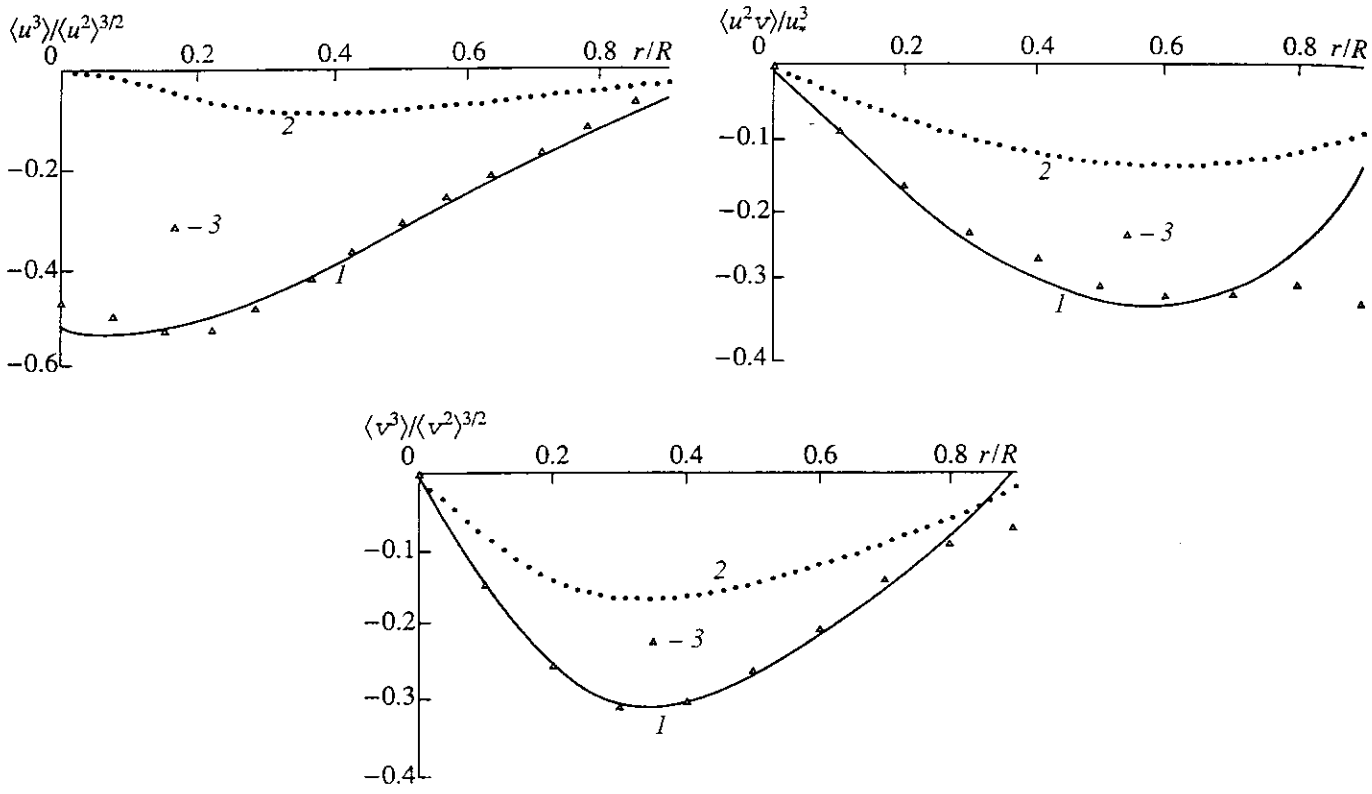

Fig. 7. Profiles of third-order moments for the velocity field with the zero value of the swirling parameter ($\Pi = 0$). Calculation: *1* – model (29), *2* – model (30), *3* – experimental data of [13, 19 - 21].

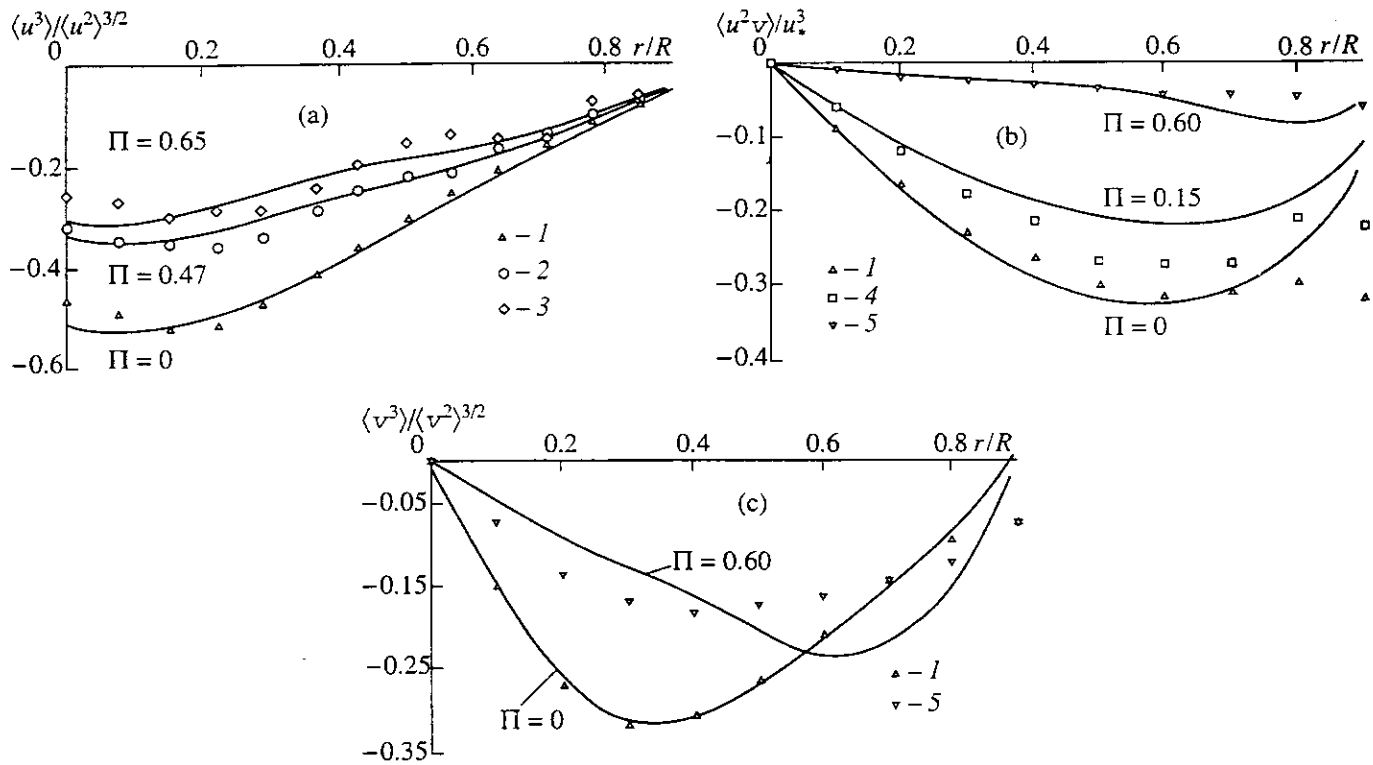

Fig. 8. Profiles of third-order moments for the velocity field in swirling flow. Solid curves - model (29). Experimental data of [13, 19 - 21]: (a) *1* – $\Pi = 0$; *2* – 0.47; *3* – 0.65; (b) *1* – $\Pi = 0$, *4* – 0.15; *5* – 0.60; (c) *1* – $\Pi = 0$, *5* – 0.60.

hypothesis, have no substantial effect on the behavior of the third-order moments, with due regard given to the approximate character of simulation of other terms in equation (24) as well. The validity of this assumption is supported by the results of comparison of the calculated profiles with the experimental data [13, 19 - 21] (Figs. 7a - 7c).

In view of relations (25) - (27), the approximate balance equation (24) takes a closed form. The resultant expression for the calculation of third moments of the velocity field may be derived from (24) in the form

$$\begin{aligned}\langle u_i u_j u_k\rangle = -c_{f3}(E/\varepsilon)\,[\,(1-c_{f1})\,(\langle u_j u_k u^m\rangle U_{i,m} \\ + \langle u_k u_i u^m\rangle U_{j,m} + \langle u_i u_j u^m\rangle U_{k,m}) \\ + c_{f2}\,(\langle u_j u_k\rangle\langle u^m u_i\rangle_{,m} + \langle u_k u_i\rangle\langle u^m u_j\rangle_{,m} \\ + \langle u_i u_j\rangle\langle u^m u_k\rangle_{,m}) + (\langle u^m u_k\rangle\langle u_i u_j\rangle_{,m} \\ + \langle u^m u_i\rangle\langle u_j u_k\rangle_{,m} + \langle u^m u_j\rangle\langle u_k u_i\rangle_{,m}) \\ - \hat{c}_{\varepsilon 3} c_{,m}(E/\varepsilon)\,[\,\langle u_k u^m\rangle g_{ij} \\ + \langle u_j u^m\rangle g_{ki} + \langle u_i u^m\rangle g_{jk}\,]\,]\,.\end{aligned} \tag{29}$$

A comparison of the results of testing of the model of third moments (29) with the experimental data yielded the following values of the empirical constant: $c_{f3} = 0.13$, $\hat{c}_{\varepsilon 3} = = 0.05$, $c_{f1} = 0.9$, and $c_{f2} = 1.0$.

Figures 7a - 7c illustrate a comparison of the experimentally obtained profiles with those calculated by the "complete" model (29) and by a simpler model derived from the local balance relation of the form

$$P_{ijk}^{(T)} + D_{ijk} + \pi_{ijk} = 0,$$

where the correlations with pressure pulsations are modeled by the simplest relaxation expression $\pi_{ijk} = -c_{f3}^{-1}(\varepsilon/E)\langle u_i u_j u_k\rangle$ in combination with the hypothesis of quasi-normality for fourth moments

$$\begin{aligned}\langle u_i u_j u_k\rangle = -c_s^* \frac{E}{\varepsilon}\,[\,\langle u_i u_j\rangle_{,m}\langle u^m u_k\rangle \\ + \langle u_j u_k\rangle_{,m}\langle u^m u_i\rangle + \langle u_i u_k\rangle_{,m}\langle u^m u_j\rangle\,]\,,\end{aligned} \tag{30}$$

$$(c_s^* = 0.13)\,.$$

One can see from the latter drawing that, for a straight round pipe, the more "complete" model (29) produces satisfactory agreement with the experiment [13, 19 - 21], while the results yielded by the commonly used model (30) fail to describe the experimental data.

In Figs. 8a - 8c, the experimental data [13, 19 - 21] are compared with the results of calculations by the "complete" model (24) for a rotating pipe flow for different swirling parameters of flow. By and large, adequate agreement is observed with the experimental data for moderately high ($\Pi \le 0.6$) swirling numbers.

CONCLUSION

The calculation results indicate that the presence of swirling of turbulent flow leads to restructuring of the flow characteristics. Suppression of turbulent pulsation characteristics of flow occurs at minor and moderate swirling of radial turbulent transfer, such as a decrease of the turbulence energy, dissipation, and turbulent stresses, mainly in the axis region. The flow parameters vary appreciably over the entire length of the rotating section ($0 \le x/R \le 50$); however, no pattern is attained that would be independent of a further increase of the distance (with respect to x) from the beginning of the rotating section.

The model of gradient transfer for third moments describes well their behavior in nonswirling flow in the central part of the channel and is in adequate agreement with the experimental data for swirling flow (as, for example, in [17] as well).

ACKNOWLEDGMENTS

This study was supported by the Russian Foundation of Fundamental Research (grant no. 94-05-16287-a).

REFERENCES

1. Onufriev, A.T. and Khristianovich, S.A., *Dokl. Akad. Nauk SSSR*, 1976, vol. 229, no. 1, p. 42.
2. Onufriev, A.T., Peculiarities of Motion in the Core of a Vortex Ring, *Fizicheskaya Mekhanika* (Physical Mechanics), Leningrad: Leningr. Gos. Univ., 1980, no. 4, p. 31.
3. Rodi, V., *Modeli Turbulentnosti Okruzhayushchei Sredy. Metody Rascheta Turbulentnykh Techenii* (Models of Turbulence of Surrounding Medium: Methods of Calculating Turbulent Flows), Moscow: Mir, 1984.
4. Kurbatskii, A.F., *Modelirovanie Nelokal'nogo Turbulentnogo Perenosa Impul'sa i Tepla* (Simulation of Non-Local Turbulent Transfer of Momentum and Heat), Novosibirsk: Nauka, 1988.
5. Launder, B.E., Reece, G.J., and Rodi, W., *J. Fluid Mech.*, 1975, vol. 68, p. 537.
6. Bradshaw, P., *J. Fluid Mech.*, 1971, vol. 36, p. 1007.
7. Londer, B.E., Priddin, S.Kh., and Sharma, B.I., *Teor. Osn. Inzh. Raschet.*, 1977, no. 1, p. 332.
8. Hossain, M.S., Mathematische Modellierung von turbulenten Auftriebstromungen, *Ph.D. Thesis*, Univ. of Karlsruhe, 1980.
9. Gibson, M.M. and Launder, B.E., *J. Fluid Mech.*, 1978, vol. 86, p. 491.
10. So, R.M.C. and Yoo, G.J., *NASA Report no. 3994*, 1986.
11. Daly, B.J. and Harlow, F.H., *Phys. Fluids*, 1970, vol. 13, no. 11, p. 2634.
12. Spalding, D.B., *GENMIX: A General Computer Program for Two-Dimensional Parabolic Phenomena*, Pergamon, 1977.
13. Zaets, P.G., Safarov, N.A., and Safarov, R.A., *Eksperimental'noe Izuchenie Povedeniya Kharakteristik Turbulentnogo Potoka pri Vrashchenii Kanala Otnositel'no*

Prodol'noi Osi. Sovremennye Problemy Mekhaniki Sploshnykh Sred (Experimental Investigation of Turbulent Flow Characteristics under Conditions of Channel Rotation about a Longitudinal Axis: Modern Problems of Continuum Mechanics), Moscow: MFTI (Moscow Physicotechnical Inst.), 1988.

14. Laufer, J., *NASA Report no. 1174*, 1954.
15. Bukreev, V.I., Zykov, V.V., and Kostomakha, V.A., *Izv. Sib. Otd. Akad. Nauk SSSR, Ser. Tekh. Nauk*, 1975, no. 13(3), p. 3.
16. Schildknecht, M., Miller, J.A., and Meier, C.E.A., *J. Fluid Mech.*, 1979, vol. 90, p. 67.
17. Panchapakesan, N.R. and Lumley, J.L., *J. Fluid Mech.*, 1993, vol. 246, p. 197.
18. Dekeyser, T. and Launder, V.E., A Comparison of Triple-Moment Temperature-Velocity Corelations in the Asymmetric Heated Jet with Alternative Closure Models, in: *Turbulent Shear Flows*, 4, Bradbury, L.J.S. *et al.*, Eds., Springer, 1983, p. 102.
19. Zaets, P.G., Onufriev, A.T., Pilipchuk, M.I., and Safarov, R.A., *Dvukhtochechnye Korrelyatsionnye Funktsii Chetvertogo Poryadka dlya Prodol'noi Skorosti v Turbulentnom Techenii vo Vrashchayushcheisya Otnositel'no Osi Trube* (Two-Point Fourth-Order Correlation Functions for Longitudinal Velocity in Turbulent Flow in a Pipe Rotating about the Axis), Available from VINITI, Moscow, 1984, no. 3831-84.
20. Pilipchuk, M.I., Investigation of Statistical Characteristics of the Longitudinal Component of Velocity of Turbulent Flow in a Rotating Pipe, *Cand. Sci. (Phys.-Math.) Dissertation*, Moscow: MFTI (Moscow Physicotech. Inst), 1986.
21. Zaets, P.G., Onufriev, A.T., Pilipchuk, M.I., and Safarov, R.A., *Odnotochechnye Momenty Prodol'noi Skorosti v Zakruchennom Turbulentnom Potoke v Trube* (One-Point Moments of Longitudinal Velocity in Swirling Turbulent Flow in a Pipe), Available from VINITI, Moscow, 1983, no. 3694-83.